Journal of Beijing Institute of Technology, 2026, Vol. 35, No. 5

Amplitude Optimization for Passive Synthetic Aperture Near-Field Grating-Lobe Suppression

Jialin Tian[1], Junhua Yang[1], Lei Song[2]✉

(1. School of Information and Electronics, Beijing Institute of Technology, Beijing 100081, China;
2. China Research Institute of Radiowave Propagation, Qingdao 266107, Shandong, China)

Abstract: To suppress high grating lobes and reduce azimuth ambiguity caused by intermittent interception of periodically scanning emitters, an element amplitude-weight optimization method is proposed. Grating-lobe suppression is formulated as an amplitude optimization problem for a block-sparse virtual array. A fitness function considering sidelobe suppression and mainlobe preservation is constructed, and an improved differential evolution algorithm is used to search for the amplitude weights. Simulation results show that the proposed method suppresses high grating lobes near the mainlobe, increases the peak-discrimination margin, and improves the localization stability of the backward projection positioning (BPP) method under sparse reception.

Keywords: spaceborne passive synthetic aperture localization; intermittent interception; grating-lobe suppression; amplitude optimization; differential evolution

1 Introduction

Passive synthetic aperture localization uses platform motion to form an equivalent aperture and estimates the emitter position through phase compensation and coherent accumulation. Direct localization can avoid error propagation caused by intermediate-parameter estimation [1], while synthetic aperture localization improves localization resolution through motion-aperture extension and coherent accumulation [2]. For spaceborne scenarios, single-satellite passive synthetic aperture localization and multi-subaperture imaging localization methods have been studied [3–5].

Practical non-cooperative radar emitters often operate in a periodic scanning mode. A spaceborne receiver can only intermittently intercept valid pulses, so the continuous observation sequence is divided into discrete data blocks. Existing studies have shown that sparse sampling can generate multiple false targets in localization images [6]. In the synthetic aperture model, intercepted positions can be regarded as along-track virtual elements, and intermittent interception forms a virtual array with nonuniform block missing, causing high grating lobes near the mainlobe of the near-field beampattern. When a grating lobe approaches the mainlobe in amplitude, noise disturbance may cause peak switching and azimuth localization ambiguity.

Sparse array synthesis provides a reference for beampattern optimization. Nonuniform arrays can change the spatial spectral structure and increase the array degrees of freedom [7], and genetic algorithms, particle swarm optimization, and differential evolution have also been used for low-sidelobe and sparse array design [8–12]. However, existing studies mainly focus on far-field beampatterns of physical antenna arrays and are difficult to apply directly to passive synthetic aperture localization with constrained element

Manuscript received May 24, 2026; revised Jul. 9, 2026; accepted Jul. 17, 2026. The associate editor coordinating the review of this manuscript was Dr. Hao Huan. This work was supported by the Stable-Support Scientific Project of China Research Institute of Radiowave Propagation (No. A240404180).

✉ Corresponding author. Email: sleimail@aliyun.com

DOI: 10.15918/j.jbit1004-0579.2026.041

positions. The optimization objective therefore shifts to the peak-discrimination reliability of the near-field beampattern.

This paper focuses on high-grating-lobe suppression under periodic scanning and intermittent interception. A near-field beampattern model for spaceborne synthetic aperture localization is established to analyze the influence of element block missing on grating-lobe formation. Then, grouped element amplitudes are used as optimization variables, and an improved differential evolution algorithm is adopted to optimize amplitude weights, suppress high grating lobes, increase the peak-discrimination margin, and reduce azimuth localization ambiguity under low-SNR conditions.

2 Near-Field Beampattern

2.1 Near-Field Model

In spaceborne passive synthetic aperture localization, satellite positions at interception instants are treated as virtual elements, and the received complex envelopes are used as element observations. With the trajectory center as the reference, a candidate point is represented by slant range R and squint angle θ, denoted by $\boldsymbol{q}(R,\theta)$. Let $\boldsymbol{p}_m$ be the satellite position at the m-th interception instant. The propagation distance is

$$r_m(R,\theta) = \left\|\boldsymbol{p}_m - \boldsymbol{q}(R,\theta)\right\|_2 \tag{1}$$

The true emitter position is denoted by $\boldsymbol{q}_0 = \boldsymbol{q}(R_0,\theta_0)$, with $r_m^{(0)} = r_m(R_0,\theta_0)$ for the m-th virtual element. Let $D = v_s T_a$ be the equivalent synthetic-aperture length, where v_s is the along-track velocity and T_a is the aperture time. The Fresnel-zone criterion is

$$R_{\mathrm{F}} = \frac{2D^2}{\lambda} \tag{2}$$

When $R_0 < R_{\mathrm{F}}$, the phase curvature across the equivalent aperture cannot be ignored, and a spherical-wave near-field response is required. Under the narrowband condition, the received signal of the m-th virtual element is written as

$$x_m = \frac{\rho_m}{r_m^{(0)}} \exp\left(-\mathrm{j}kr_m^{(0)}\right) + n_m \tag{3}$$

where ρ_m is a slowly varying complex coefficient, $1/r_m^{(0)}$ represents the spherical-wave amplitude attenuation, n_m is the received noise, $k = 2\pi f_c/c$ is the wavenumber, and f_c is the carrier frequency. Eq. (3) retains the range-dependent amplitude attenuation and spherical-wave phase term, and is suitable for near-field array-response modeling [13].

For a candidate point $\boldsymbol{q}(R,\theta)$, phase compensation and coherent accumulation are performed according to the theoretical distances to all elements. The near-field beampattern is defined as

$$P(R,\theta) = \left|\sum_{m=1}^{M} \frac{x_m}{r_m(R,\theta)} \exp\left(\mathrm{j}kr_m(R,\theta)\right)\right|^2 \tag{4}$$

When the candidate point coincides with the true target position, $r_m(R,\theta)$ matches $r_m^{(0)}$, and the compensated residual phases are approximately aligned, forming the main peak. Therefore, the emitter position estimate is given by

$$(\widehat{R},\widehat{\theta}) = \underset{(R,\theta)\in\Omega}{\arg\max}\, P(R,\theta) \tag{5}$$

Eq. (5) shows that spaceborne passive synthetic aperture localization can be regarded as a peak-search process over the near-field beampattern of the virtual array, while sidelobe and grating-lobe levels outside the mainlobe affect peak-discrimination reliability.

2.2 Intermittent Interception

For a periodically scanning emitter, the spaceborne receiver intercepts valid pulses only when the beam sweeps nearby. Let $w_m = w(t_m)$ be the receiving-gate value at the m-th interception instant. The signal used for beampattern synthesis is

$$\tilde{x}_m = w_m x_m \tag{6}$$

where $\tilde{x}_m$ is the m-th received signal after intermittent interception, and $w_m \in \{0,1\}$ indicates whether the pulse is retained. Thus, intermittent interception is equivalent to selecting along-track

virtual elements, converting the continuous virtual array into a block-sparse array.

In practical scanning, $w(t)$ is affected by the scan period T_c, antenna pattern, propagation loss, and detection threshold. Within one scan period, the effective receiving interval usually contains several blocks with different centers and durations. The receiving-gate function can then be written as

$$w(t)=\sum_{p=-\infty}^{+\infty}\sum_{l=1}^{L}\operatorname{rect}\left(\frac{t-pT_c-t_l}{T_l}\right) \tag{7}$$

where p is the scan-period index, L is the number of effective receiving blocks, and t_l and T_l are the center time and duration of the l-th block. Eq. (7) indicates a nonuniform multi-block receiving window. This window corresponds to the block-sparse virtual array shown in Fig. 1.

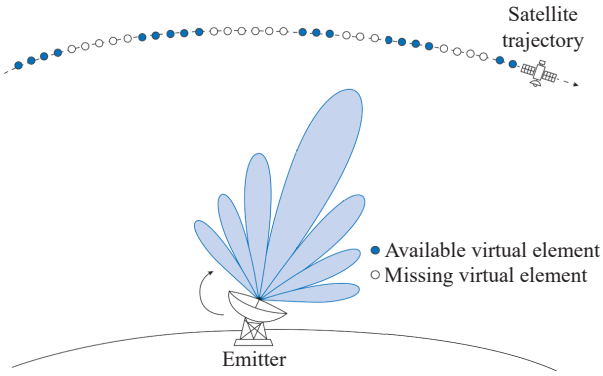


Fig. 1 Schematic of the block-sparse virtual array

2.3 Grating-Lobe Formation

From Eqs. (6) and (7), periodic intermittent interception is equivalent to time gating of the ideal received signal, whose frequency-domain form follows from the convolution relation [14]. Let $W(f)$ be the Fourier transform of $w(t)$. Since $w(t)$ has period T_c, its spectrum consists of discrete spectral lines with spacing $1/T_c$ and is written as

$$W(f)=\frac{1}{T_c}\sum_{n=-\infty}^{+\infty}A_n\delta\left(f-\frac{n}{T_c}\right) \tag{8}$$

where n is the spectral-line order, and A_n is the amplitude coefficient of the n-th spectral line. For the nonuniform block receiving function in Eq. (7), the spectral-line coefficient is written as

$$A_n=\sum_{l=1}^{L}T_l\operatorname{sinc}\left(\frac{nT_l}{T_c}\right)\exp\left(-\mathrm{j}2\pi n\frac{t_l}{T_c}\right) \tag{9}$$

Eq. (9) shows that A_n is determined by the block duration T_l and center time t_l. Nonuniform blocks make A_n fluctuate and thus change the amplitudes of different spectral replicas.

Let $S(f)$ be the spectrum of the continuous received signal, and $S_{\text{int}}(f)$ be the spectrum after intermittent interception. Then the spectrum after intermittent interception is written as

$$S_{\text{int}}(f)=S(f)*W(f)=\frac{1}{T_c}\sum_{n=-\infty}^{+\infty}A_nS\left(f-\frac{n}{T_c}\right) \tag{10}$$

The spectral replication process in Eqs. (8)–(10) is shown in Fig. 2. Eq. (10) indicates that the original spectrum is replicated at intervals of $1/T_c$, with amplitudes modulated by A_n, and appears as azimuth grating lobes in the near-field beampattern.

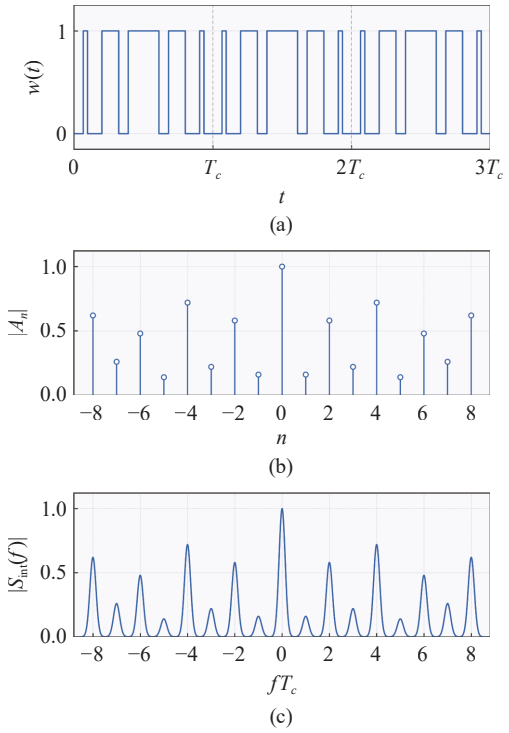


Fig. 2 Schematic of spectral replicas: (a) receiving gate $w(t)$; (b) spectral-line coefficients $|A_n|$; (c) replicated spectrum $|S_{\text{int}}(f)|$

Near the mainlobe, the Doppler–squint mapping can be approximated by the equivalent

along-track velocity v_s, giving the adjacent grating-lobe spacing as

$$\Delta\theta \approx \arcsin\left(\frac{\lambda}{v_s T_c}\right) \tag{11}$$

Thus, nonuniform block missing may produce local high grating lobes. Since virtual element positions are difficult to adjust, the following section uses amplitude weighting for suppression.

3 Amplitude Optimization

3.1 Optimization Variables

For the block-sparse array formed by intermittent interception, element-amplitude optimization can be viewed as applying adjustable time-domain weights to the single-period receiving window. This changes the window spectrum and the spectral-line coefficients A_n, thereby regulating grating-lobe amplitudes in the near-field beampattern.

To reduce the optimization dimension, element amplitudes are grouped. The available along-track elements are divided into G groups, and elements in the same group share one amplitude coefficient. Let $g(m)$ be the group index of the m-th element, and $a_{g(m)}$ the corresponding group amplitude. The optimized near-field beampattern is

$$P_{\boldsymbol{a}}(R,\theta) = \left|\sum_{m=1}^{M} a_{g(m)} \frac{\tilde{x}_m}{r_m(R,\theta)} \exp\left(\mathrm{j}k r_m(R,\theta)\right)\right|^2 \tag{12}$$

where $\tilde{x}_m$ is the intermittently intercepted signal defined in Eq. (6), and $r_m(R,\theta)$ is the propagation distance from the candidate point to the m-th element. When all $a_{g(m)} = 1$, Eq. (12) reduces to the unoptimized beampattern. With different group weights, element contributions are redistributed, changing the grating-lobe and sidelobe amplitudes outside the mainlobe.

3.2 Fitness Function

Nonuniform block missing produces high grating lobes and strong sidelobes in the near-field beampattern, reducing the amplitude margin between the mainlobe and interference peaks and degrading peak-discrimination reliability. To balance high-grating-lobe suppression, overall sidelobe control, and mainlobe-resolution preservation, a composite fitness function is constructed to evaluate the beampattern quality of each candidate amplitude distribution.

Let the grouped amplitude vector be $\boldsymbol{a} = [a_1, a_2, \ldots, a_G]^{\mathrm{T}}$, whose beampattern is given by Eq. (12). The fitness function is defined as

$$J(\boldsymbol{a}) = \alpha_1 F_{\mathrm{PSLR}} + \alpha_2 F_{\mathrm{TopK}} + \alpha_3 F_{\mathrm{ISL}} + \lambda_b F_{\mathrm{BW}} \tag{13}$$

To specify the terms in Eq. (13), the azimuth slice $P_{\boldsymbol{a}}(R_p,\theta)$ at the main-peak slant range R_p is normalized as

$$\widetilde{P}_{\boldsymbol{a}}(\theta) = \frac{P_{\boldsymbol{a}}(R_p,\theta)}{P_{\boldsymbol{a}}(R_p,\theta_p)} \tag{14}$$

where θ_p is the mainlobe-peak angle, and Ω_s denotes the sidelobe region outside the mainlobe. The three sidelobe metrics are

$$F_{\mathrm{PSLR}} = \max_{\theta\in\Omega_s} \widetilde{P}_{\boldsymbol{a}}(\theta) \tag{15}$$

$$F_{\mathrm{TopK}} = \frac{1}{K}\sum_{k=1}^{K} \widetilde{P}_{(k)} \tag{16}$$

$$F_{\mathrm{ISL}} = \frac{1}{N_s}\sum_{\theta_i\in\Omega_s} \left[\widetilde{P}_{\boldsymbol{a}}(\theta_i)\right]^2 \tag{17}$$

where $\widetilde{P}_{(k)}$ is the k-th largest local peak in Ω_s, and N_s is the number of samples in Ω_s. Here, F_{PSLR}, F_{TopK}, and F_{ISL} evaluate the highest sidelobe, strong-sidelobe average, and sidelobe-region energy, respectively. The mainlobe-width penalty is

$$F_{\mathrm{BW}} = \left[\max\left(0, \frac{B_{\boldsymbol{a}}}{B_0} - 1\right)\right]^2 \tag{18}$$

where $B_{\boldsymbol{a}}$ and B_0 are the -3 dB mainlobe widths of the optimized and unoptimized azimuth slices, respectively.

The coefficient settings in Eq. (13) are listed in Tab. 1 and kept fixed in all experiments.

Tab. 1 Parameter settings in the fitness function

Parameter	Value
α_1	0.24
α_2	0.18
α_3	0.18
λ_b	0.03
K	6

Thus, minimizing $J(\boldsymbol{a})$ suppresses sidelobes while preserving the mainlobe width, thereby improving azimuth peak discrimination.

3.3 Improved Differential Evolution

From Eq. (13), amplitude optimization is a continuous nonlinear search problem. The fitness function is built from near-field beampattern metrics and is multimodal and non-analytic. Differential evolution has a simple structure and few parameters, making it suitable for continuous global optimization [15]. Therefore, it is used as the baseline method for amplitude-weight optimization.

To reduce search-direction fluctuation and local stagnation in the iterative process, three modifications are introduced: mutation strategy, parameter feedback, and stagnation handling. First, better individuals are used to guide random differential mutation, so that the population moves toward low-fitness regions while retaining random exploration. Second, the scaling factor F and crossover probability C_r are adjusted using successful-update feedback, maintaining a broad search range in the early stage and enhancing local search in the later stage. Finally, when the best fitness shows no obvious decrease for several generations, elite individuals are retained and part of the poorer individuals are randomly perturbed to restore population diversity. Existing studies show that F and C_r affect the search behavior of differential evolution, and adaptive parameter adjustment improves its adaptability at different optimization stages [16].

Successful F and C_r values are stored in $S_F^{(t)}$ and $S_{C_r}^{(t)}$ after parent replacement. The centers are updated as

$$\mu_F^{(t+1)} = (1-\rho)\mu_F^{(t)} + \rho\frac{\sum_{F\in S_F^{(t)}} F^2}{\sum_{F\in S_F^{(t)}} F + \varepsilon} \tag{19}$$

$$\mu_{C_r}^{(t+1)} = (1-\rho)\mu_{C_r}^{(t)} + \rho\,\mathrm{mean}\left(S_{C_r}^{(t)}\right) \tag{20}$$

where ρ is the feedback factor and ε avoids division by zero. If no successful update occurs, the centers remain unchanged.

The stagnation counter is updated by

$$s^{(t)} = \begin{cases} 0, & J_{\text{best}}^{(t)} < J_{\text{best}}^{(t-1)} - \varepsilon_s \\ s^{(t-1)} + 1, & \text{otherwise} \end{cases} \tag{21}$$

When $s^{(t)} \geqslant G_{\text{stall}}$, poorer individuals are perturbed as

$$\boldsymbol{a}_i^{(t+1)} = \Pi_{[0,a_{\max}]}\left(\boldsymbol{a}_e^{(t)} + \sigma_r a_{\max}\boldsymbol{q}_i^{(t)}\right), \quad i \in \mathcal{W}^{(t)} \tag{22}$$

Here, $\boldsymbol{a}_e^{(t)}$ is randomly selected from the elite set $\mathcal{E}^{(t)}$, which contains the top p_e fraction of the population; $\mathcal{W}^{(t)}$ denotes the poorer individuals; $\boldsymbol{q}_i^{(t)}$ is zero-mean; and $\Pi_{[0,a_{\max}]}$ denotes amplitude clipping. The parameter values are $\mu_F^{(0)} = 0.68$, $\mu_{C_r}^{(0)} = 0.88$, $\rho = 0.10$, $\varepsilon_s = 10^{-6}$, $G_{\text{stall}} = 18$, $\sigma_r = 0.12$, $a_{\max} = 10$, $p_e = 0.12$.

Based on these strategies, the amplitude optimization procedure is shown in Algorithm 1. Each individual represents a candidate grouped amplitude-weight vector $\boldsymbol{a}$, and its fitness is calculated by Eq. (13).

Algorithm 1: Improved DE-based array amplitude optimization procedure

Input: Virtual element positions $\{\boldsymbol{p}_m\}_{m=1}^M$, intermittently intercepted signals $\{\tilde{x}_m\}_{m=1}^M$, search region Ω, group mapping $g(m)$, amplitude-weight range $[a_{\min}, a_{\max}]$, population size N_p, maximum iterations $G_{\max}$.

Output: Optimal grouped amplitude weight $\boldsymbol{a}^*$, optimized near-field beampattern $P_{\boldsymbol{a}^*}(R,\theta)$.

1: Initialize the population $\{\boldsymbol{a}_i^0\}_{i=1}^{N_p}$, parameter centers $\mu_F^{(0)}$ and $\mu_{C_r}^{(0)}$, and stagnation counter $s^{(0)} = 0$;

2: Compute $P_{\boldsymbol{a}_i}(R,\theta)$ and $J(\boldsymbol{a}_i)$ using Eqs. (12) and (13);

3: **for** $t = 1, 2, \ldots, G_{\max}$ **do**

4: Set $S_F^{(t)} = \varnothing$ and $S_{C_r}^{(t)} = \varnothing$;

5: Generate $F_i^{(t)}$ and $C_{r,i}^{(t)}$ from the current parameter centers;

6: Generate mutant vectors using random differential mutation and better-individual guidance;

7: Generate trial individuals according to $C_{r,i}^{(t)}$;

8: Compute the beampattern and fitness of each trial individual using Eqs. (12) and (13);

9: If a trial individual has a smaller fitness, replace its parent and store $F_i^{(t)}$ and $C_{r,i}^{(t)}$ in $S_F^{(t)}$ and $S_{C_r}^{(t)}$;

10: Update μ_F and μ_{C_r} using Eqs. (19) and (20);

11: Update $s^{(t)}$ using Eq. (21);

12: If $s^{(t)} \geq G_{\text{stall}}$, retain elite individuals and perturb poorer individuals using Eq. (22);

13: **end for**

14: Select the individual with the smallest fitness as $\boldsymbol{a}^*$;

15: Substitute $\boldsymbol{a}^*$ into Eq. (12) to obtain $P_{\boldsymbol{a}^*}(R,\theta)$.

4 Simulation Results

4.1 Simulation Setup

To verify the sidelobe-suppression performance under intermittent interception, a spaceborne passive synthetic aperture localization simulation is conducted. The same near-field beampattern search region, receiving-block structure, and evaluation criteria are used before and after optimization. The main parameters are listed in Tab. 2.

The peak sidelobe ratio (PSLR) is defined as the amplitude difference between the mainlobe peak and the highest sidelobe outside the mainlobe. A larger PSLR indicates a lower highest sidelobe relative to the mainlobe and a larger peak-discrimination margin. The following results are calculated from the complete near-field beampattern, and the optimization effect is illustrated by the azimuth slice near the main-peak slant range.

Tab. 2 Main simulation parameters

Parameter	Value
Carrier frequency	3 GHz
Wavelength	0.1 m
Orbital altitude	500 km
Nominal slant range	1000 km
Along-track velocity	7.62 km/s
Synthetic aperture time	3 s
Pulse repetition interval	0.5 ms
SNR	−10 dB
Scan period	0.5 s
Receiving duty cycle	35%–50%
Number of amplitude variables	180
Population size	130
Maximum iterations	100

4.2 Algorithm Comparison

To verify the effectiveness of the improved differential evolution algorithm in amplitude optimization, it is compared with the genetic algorithm, particle swarm optimization, and classical differential evolution. The four algorithms use the same optimization variables, search range, and fitness function, and all minimize Eq. (13) under the same maximum number of iterations. Fig. 3 shows the fitness convergence curves, and Tab. 3 presents the optimization results.

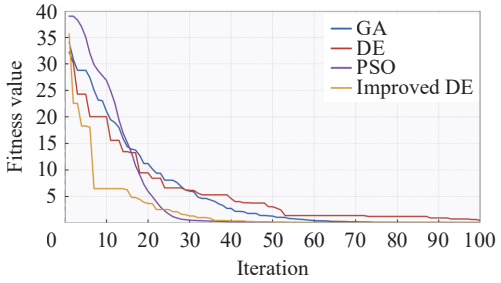


Fig. 3 Fitness convergence curves of different algorithms

As shown in Fig. 3 and Tab. 3, all four algorithms reduce the fitness value. Compared with GA, PSO, and classical DE, the improved DE converges faster in the early stage, obtains the lowest final fitness, and achieves the highest optimized PSLR. Its runtime is of the same order as those of the compared algorithms, indicating that the improved DE is more suitable for the amplitude-weight optimization problem with acceptable computational cost.

4.3 Grating-Lobe Suppression

The 40% receiving-duty-cycle case is selected as a representative scenario. Fig. 4 compares the azimuth slices before and after array amplitude

Tab. 3 Optimization results of different algorithms

Metric	GA	PSO	Classical DE	Improved DE
Fitness at iteration 20	11.190612	5.959961	9.448224	3.655728
Fitness at iteration 50	1.284233	0.155675	3.054827	0.204439
Final fitness	0.090691	0.048949	0.470836	0.009929
Optimized PSLR (dB)	9.615	9.719	9.431	10.102
Runtime (s)	497.8313	470.6658	460.5563	473.2202

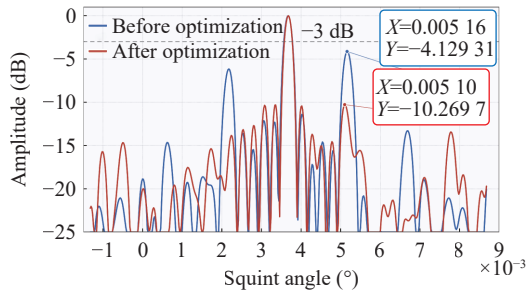


Fig. 4 Azimuth-slice comparison before and after optimization

optimization.

As shown in Fig. 4, before optimization, distinct high sidelobes appear near the mainlobe. The PSLR is 4.129 dB, indicating a small amplitude margin between the mainlobe and the highest sidelobe outside the mainlobe. After grouped amplitude-weight optimization, the high sidelobes on both sides of the mainlobe are significantly reduced, and the PSLR increases to 10.270 dB, with an improvement of 6.141 dB. Meanwhile, no obvious mainlobe broadening is observed after optimization.

These results show that the proposed method suppresses local high sidelobes while preserving the mainlobe, improves the PSLR, and increases the peak-discrimination margin. As a result, the probability of peak switching under noise disturbance is reduced, which helps mitigate azimuth localization ambiguity.

4.4 Localization Stability Analysis

To evaluate localization stability under different receiving duty cycles, Monte Carlo simulations are conducted for the 35%–50% duty-cycle cases. The RMSE is used to measure the localization error and is defined as

$$\mathrm{RMSE}=\sqrt{\frac{1}{N}\sum_{i=1}^{N}e_i^2} \tag{23}$$

where N is the number of Monte Carlo trials, and e_i is the localization error in the i-th trial. Fig. 5 compares the RMSE and PSLR before and after optimization under different receiving duty cycles.

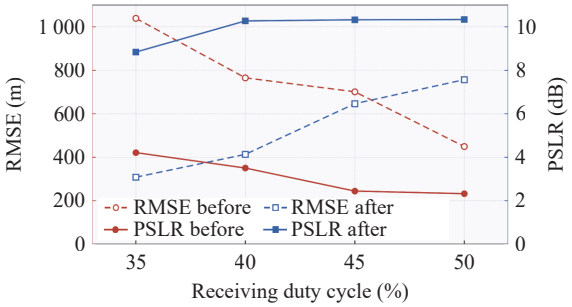


Fig. 5 Comparison of RMSE and PSLR under different receiving duty cycles

As shown in Fig. 5, the PSLR is improved after optimization for all duty-cycle cases, and the RMSE is lower than that before optimization. This indicates that amplitude-weight optimization increases the peak-discrimination margin and reduces the localization error. At the 35% duty cycle, the RMSE decreases from 1039 m to 421 m. For the 40%–50% cases, the optimized PSLR remains around 10 dB, and the RMSE is maintained within 232–350 m. These results show that the proposed method improves the PSLR, effectively reduces the probability of peak misidentification under noise disturbance, and enhances the localization stability of the BPP method under sparse reception.

5 Conclusion

This paper formulates high-grating-lobe suppression under intermittent interception as an amplitude optimization problem for a block-sparse virtual array, and uses an improved differential evolution algorithm to optimize element amplitude

weights. Simulation results show that the proposed method suppresses high grating lobes near the mainlobe, increases the peak-discrimination margin, and reduces the optimized RMSE. These results indicate that the method reduces peak misidentification under noise disturbance and improves the localization stability of the BPP method under sparse reception.

References:

[1] A. J. Weiss,"Direct geolocation of wideband emitters based on delay and Doppler," *IEEE Transactions on Signal Processing*, vol. 59, no. 6, pp. 2513-2521, 2011.

[2] G. Sun, W. Dong, Y. Wang, and M. Xing,"Synthetic aperture positioning: A review," *Journal of Beijing Institute of Technology*, vol. 33, no. 2, pp. 89-102, 2024.

[3] A. Li, H. Huan, R. Tao, and L. Zhang,"Passive synthetic aperture high-precision radiation source location by single satellite," *IEEE Geoscience and Remote Sensing Letters*, vol. 19, pp. 1-5, 2022.

[4] L. Zhang, H. Huan, R. Tao, and Y. Wang,"Emitter localization algorithm based on passive synthetic aperture," *IEEE Transactions on Aerospace and Electronic Systems*, vol. 58, no. 4, pp. 2687-2701, 2022.

[5] J. Yang, H. Huan, and R. Tao,"Multisubaperture backward projection positioning algorithm for radiation sources by single satellite," *IEEE Transactions on Aerospace and Electronic Systems*, vol. 61, no. 2, pp. 1267-1282, 2025.

[6] J. Sun, H. Huan, R. Tao, and Y. Wang,"A passive synthetic aperture localization method based on sparse sampling reconstruction," *IEEE Geoscience and Remote Sensing Letters*, vol. 22, pp. 1-5, 2025.

[7] P. Pal and P. P. Vaidyanathan,"Nested arrays: A novel approach to array processing with enhanced degrees of freedom," *IEEE Transactions on Signal Processing*, vol. 58, no. 8, pp. 4167-4181, 2010.

[8] R. L. Haupt,"Thinned arrays using genetic algorithms," *IEEE Transactions on Antennas and Propagation*, vol. 42, no. 7, pp. 993-999, 1994.

[9] M. M. Khodier and C. G. Christodoulou,"Linear array geometry synthesis with minimum sidelobe level and null control using particle swarm optimization," *IEEE Transactions on Antennas and Propagation*, vol. 53, no. 8, pp. 2674-2679, 2005.

[10] D. G. Kurup, M. Himdi, and A. Rydberg,"Synthesis of uniform amplitude unequally spaced antenna arrays using the differential evolution algorithm," *IEEE Transactions on Antennas and Propagation*, vol. 51, no. 9, pp. 2210-2217, 2003.

[11] C. Lin, A. Qing, and Q. Feng,"Synthesis of unequally spaced antenna arrays by using differential evolution," *IEEE Transactions on Antennas and Propagation*, vol. 58, no. 8, pp. 2553-2561, 2010.

[12] R. Zhang, Y. Zhang, J. Sun, and Q. Li,"Pattern synthesis of linear antenna array using improved differential evolution algorithm with SPS framework," *Sensors*, vol. 20, no. 18, pp. 5158, 2020.

[13] H. L. Van Trees, *Optimum Array Processing: Part IV of Detection, Estimation, and Modulation Theory*. New York, NY, USA: John Wiley & Sons, 2002.

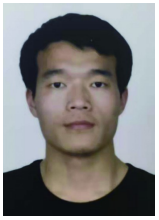
[14] A. V. Oppenheim and R. W. Schafer, *Discrete-Time Signal Processing*. 3 rd ed. Upper Saddle River, NJ, USA: Pearson, 2010.

[15] R. Storn and K. Price,"Differential evolution - a simple and efficient heuristic for global optimization over continuous spaces," *Journal of Global Optimization*, vol. 11, no. 4, pp. 341-359, 1997.

[16] J. Brest, S. Greiner, B. Boskovic, M. Mernik, and V. Zumer,"Self-adapting control parameters in differential evolution: A comparative study on numerical benchmark problems," *IEEE Transactions on Evolutionary Computation*, vol. 10, no. 6, pp. 646-657, 2006.



Jialin Tian is with the School of Information and Electronics, Beijing Institute of Technology, Beijing, China. His research interests include passive localization and array signal processing.



Junhua Yang received the B.E. degree in electronic information engineering from Beijing Institute of Technology, Beijing, China, in 2019. He is currently working toward the Ph.D. degree in information and communication engineering with Beijing Institute of Technology, Beijing, China.



Lei Song is a professor-level senior engineer with the China Research Institute of Radiowave Propagation, Qingdao, China. His research interests include radio detection and electronic information system design.